

1 **Title page**

2

3 **Multi-omics correlates of insulin resistance and circadian function**
4 **mapped directly from human serum**

5

6 Ngoc-Hien Du^{1*}, Flore Sinturel^{2, 3, 4, 5}, Nora Nowak⁶, Pauline Gosselin^{2, 3, 4, 5, 7},
7 Camille Saini^{2, 3, 4, 5, 7}, Idris Guessous⁷, François R. Jornayvaz^{9, 5}, Jacques
8 Philippe^{9, 5}, Guillaume Rey^{4, 5, 8}, Emmanouil T. Dermitzakis^{4, 5, 8}, Renato
9 Zenobi⁶, Charna Dibner^{2, 3, 4, 5}, and Steven A. Brown¹

10 ¹Institute of Pharmacology and Toxicology, University of Zurich, 8057 Zurich,
11 Switzerland.

12 ²Department of Surgery, Division of Thoracic and Endocrine Surgery,
13 University Hospitals of Geneva, 1211 Geneva, Switzerland.

14 ³Department of Cell Physiology and Metabolism, Faculty of Medicine,
15 University of Geneva, 1211 Geneva, Switzerland.

16 ⁴Institute of Genetics and Genomics of Geneva (iGE3), 1211 Geneva,
17 Switzerland.

18 ⁵Diabetes Center, Faculty of Medicine, University of Geneva, 1211 Geneva,
19 Switzerland.

20 ⁶Department of Chemistry and Applied Biosciences, ETH Zurich, 8093 Zurich,
21 Switzerland.

22 ⁷Department and Division of Primary Care Medicine, University Hospitals of
23 Geneva, 1211 Geneva, Switzerland.

24 ⁸Department of Genetic Medicine and Development, Faculty of Medicine,
25 University of Geneva, Geneva, Switzerland.

26 ⁹Department of Medicine, Division of Endocrinology, Diabetes, Nutrition, and
27 Therapeutic Education of Patient, University Hospitals of Geneva, 1211
28 Geneva, Switzerland.

29 *Correspondance: Ngoc-Hien Du, hiendngoc@gmail.com, ORCID iD: 0009-
30 0007-3525-8094.

31

32 Present address: Ngoc-Hien Du, Laboratory for Biomedical Microfluidics,
33 Swiss Federal Institute of Technology Lausanne (EPFL), Rue du Bugnon 25A,
34 1005 Lausanne, Switzerland.

35 **Keywords: GWAS, circadian rhythms, obesity and type 2 diabetes,**
36 **insulin resistance, serum metabolomics, chronotype**

37

38 **Acknowledgements:** S.A.B, C.D., I.G., J.P., F.R.J., R.Z., and E.T.D.
39 designed the study. P.G, C.S., I.G., F.R.J., and J.P. conducted subject
40 enrolment and sampling. F.S. and P.G. carried out cell culture experiments.
41 N.N. performed the mass spectrometry measurements and the corresponding

data processing. NH.D, PG and FS performed DNA, and RNA extractions. NH.D. and G. R. carried out the GWAS analysis. NH.D., N. N., and F.S. carried out the combined data analysis and wrote the manuscript with input from all co-authors. The authors thank Dr. A. Biancolin, Dr. M. Sato, and Dr. A. Autour for scientific discussions and critical reading of the manuscript; Drs. G. Gastaldi, M. Mavromati and M. Portella for help with the patient recruitment; Mrs. N. Francioli for assistance with the collection of blood samples and cutaneous biopsies.

Funding information: The work in the groups of S.A.B., E.T.D. and J.P. was funded by SNSF Synergia grant number CRSII3_160741. C.D. received funding from the SNSF grants 31003A_166700/1 and 310030-184708, the Vontobel Foundation, the Olga Mayenfisch Foundation, the Novartis Foundation for Medical-Biological Research, EFSD/Novonordisk Programme for Diabetes Research in Europe, Leenaards Foundation, Gerthrud-Meissner Foundation, the Fondation Ernst et Lucie Schmidheiny, the Jubiläumsstiftung Swiss Life Foundation, Velux Foundation, Swiss Cancer League, and ISREC Foundation. F.S. received funding from the Young Independent Investigator Grant SGED/SSSED.

Data availability statement: Genotype data was deposited at 10.5281/zenodo.10598274. Metabolomic data was deposited at 10.5281/zenodo.10605035.

Conflict of interest disclosure: Emmanouil T. Dermitzakis is a GSK employee; this work was performed before he joined GSK. Guillaume Rey is an employee of Unilabs; this work was done before he joined Unilabs.

Patient consent and ethical approval statement: All participants gave informed consent and the study had ethics committee approval (CER11-015). The study was registered at ClinicalTrials.gov (registration no. NCT02384148).

Abstract

While it is generally known that metabolic disorders and circadian dysfunction are intertwined, how the two systems affect each other is not well understood, nor are the genetic factors that might exacerbate this pathological interaction. Blood chemistry is profoundly changed in metabolic disorders, and we have previously shown that serum factors change cellular clock properties. To investigate if circulating factors altered in metabolic disorders have circadian modifying effects, and whether these effects are of genetic origin, we measured circadian rhythms in U2OS cell in the presence of serum collected from diabetic, obese, or control subjects. We observed that circadian period lengthening in U2OS cells was associated with serum chemistry that is characteristic of insulin resistance. Characterizing the genetic variants that altered circadian period length by genome-wide association analysis, we found that one of the top variants mapped to the E3 ubiquitin ligase MARCH1 involved in insulin sensitivity. Confirming our data, the serum circadian modifying variants were also enriched in type 2 diabetes and chronotype variants identified in the UK Biobank cohort. Finally, to identify serum factors that might be involved in period lengthening, we performed detailed metabolomics, and found that the circadian modifying variants are particularly associated with branched chain amino acids, whose levels are known to correlate with diabetes and insulin resistance. Overall, our multi-omics data showed comprehensively that systemic factors serve as a path through which metabolic disorders influence circadian system, and these can be examined in human populations directly by simple cellular assays in common cultured cells.

Introduction

In virtually all light-sensitive organisms, circadian clocks govern most aspects of physiology¹, to synchronize them with the environment². Rodent as well as human studies suggest that there is bidirectional cross talk between clocks and metabolism³. In mice, while circadian misalignment between meal time and light-dark cycle leads to disruption of metabolic pathways⁴⁻⁶, high fat diet induces the alteration of circadian oscillations⁷. Combination of circadian misalignment and high fat diet led to further worsening of metabolic outcome^{8,9}. In humans, molecular circadian oscillations in islets are dampened upon type 2 diabetes (T2D), concordant with disrupted insulin and glucagon rhythms¹⁰. In addition, physiological rhythms such as body temperature and heart rate are also disrupted in diabetic patients¹¹. Conversely, numerous studies show that circadian misalignment has direct consequences on metabolic outcomes^{12,13}.

T2D patients exhibit hyperglycemia, hyperinsulinemia, and dyslipidemia^{14,15}, with the blood metabolome and proteome undergoing profound alterations¹⁶. Among blood metabolites, branched-chain amino acids (BCAA) are the most consistently associated with obesity and insulin resistance, two hallmarks of T2D¹⁷. Noteworthy, we have demonstrated that aging-associated serum factors, whose identities are yet to be established, led to shortened circadian period length and advanced phases in primary skin fibroblasts derived from the same individuals¹⁸. In addition, in a small cohort of T2D subjects,

individual differences in serum glycated hemoglobin (HbA_{1c}) were inversely associated with the circadian period length of primary skin fibroblasts' oscillations when the cellular clocks were measured in the presence of the corresponding patient serum¹⁹.

Therefore, we hypothesized that altered metabolic signatures in serum of patients bearing metabolic diseases such as obesity and T2D might have circadian rhythm modifying effects. In this study, we used a combinatorial approach of genomic and metabolomic association to gain insights into molecular factors in serum that modify circadian period length in metabolically compromised patients.

Materials and Methods

Participant characteristics and study design

Three hundred fourteen participants were enrolled in this study, dubbed the Diachron cohort, 274 of which met inclusion - exclusion criteria listed in Table S1 and Table S2. Age- and sex- matched study participants belonged to four categories: normoglycemic non-diabetic non-obese (referred to as control subjects in this study), normoglycemic non-diabetic obese (referred to as obese non-T2D subjects), obese with T2D (referred to as obese T2D subjects), and non-obese with T2D (referred to as non-obese T2D subjects). Obesity was defined by body mass index (BMI) > 30; T2D - by glycated hemoglobin (HbA_{1c}) > 6.5% (equivalent to 48 mmol/mol). A list of the baseline characteristics of the participants in each group is presented in Table 1. All participants gave informed consent, and the study had ethics committee approval (CER11-015), and was registered at ClinicalTrials.gov (registration no. NCT02384148). All study participants filled out the Munich Chronotype Questionnaire (MCTQ), allowing calculation of MSF_{sc} values that characterize an individual's chronotype. The participants were asked to follow a moderate diet without excess fat or alcohol intake, 24 hours prior to the testing day.

Harvesting of sera

Blood samples for all study participants were collected between 08:00 am and 10:00 am, following overnight fasting from 10 pm. Blood samples were collected in clot-activator vacutainers and immediately analyzed by the Geneva University Hospital laboratory for blood glucose, HbA_{1c}, hormones, lipids, liver and kidney functions (detailed list of the measured blood clinical parameters is reported in Table S3). Serum was immediately prepared from blood samples by centrifugation (10 min, 1650 x g, 4 °C) and stored at -80 °C for further analyses.

Primary dermal fibroblast culture, in vitro synchronization and DNA extraction

Cutaneous biopsies were taken from each participant's shoulder between 8:00 am and 10:00 am and processed as described previously²⁰. Cells in culture were synchronized with a 30-minute 100 nM dexamethasone pulse,

and collected 24 h later. DNA was extracted using QIAamp DNA Mini Kit (Qiagen AG, Cat# 51304) and eluted in a final volume of 15 µL.

Lentivector production

Bmal1-luciferase lentiviral particles²¹ were produced at the Viral Vector Facility of the University of Zurich. Transient transfection in 293T cells was performed using the polyethylenimine method²⁰. Lentiviral particles were harvested at 48 h post-transfection, PEG precipitated, titred, and used for the transduction of the U2OS cells with multiplicity of infection (MOI) of 3.

U2OS cell culture, in vitro synchronization and real-time bioluminescence recording

U2OS cells (ATCC, Cat# HTB-96, RRID:CVCL_0042) were cultured in DMEM low glucose (GIBCO) supplemented with 1% Penicillin/Streptomycin (GIBCO, Cat# 15140122), 0.5% Amphotericin B (Sigma, Cat# A2942), 0.5% Gentamycin (Sigma, Cat# G1397) and 10% FCS (GIBCO, Cat# A5256701). Cells were transduced with lentivirus expressing *Bmal1-luciferase*, and selected with Blasticidin S (Gibco, Cat# R21001) at 25 µg/ml final concentration. The same batch of transduced U2OS cells was used for all the circadian measurements. After synchronization of the cells with a 30-min pulse of 100 nmol/l dexamethasone, the circadian bioluminescence recording was performed in DMEM low glucose without phenol red (GIBCO, Cat# 31053028) supplemented with 1% Penicillin/Streptomycin (GIBCO, Cat# 15140122), 0.5% Amphotericin B (Sigma, Cat# A2942), 0.5% Gentamycin (Sigma, Cat# G1397), 1 mmol/l of luciferin and in the presence of 10% of the individual's sera. Bioluminescence was monitored by a home-made robotic device equipped with photomultiplier tube detector assemblies, allowing the recording of technical triplicates in 24-well plates for 1 week. After removing the first oscillation cycle, to avoid a potential bias stemming from the immediate early response to synchronization, raw data were processed by moving average with a window of 24 h, allowing to subtract the baseline and analyze the time series without the variability of magnitudes.

Metabolomics by UPLC-MS

Sample preparation and measurements

200 µL of serum were thawed on ice, 200 µL of 1 mg/mL ¹⁵N₂-tryptophan (Cambridge Isotope Laboratories, Inc., Tewksbury, USA) in water (LC-MS grade, Fisher Scientific, Pittsburgh, USA) were added as internal standard, and proteins were precipitated by the addition of 600 µL of methanol (LC-MS grade, Fisher Scientific, Pittsburgh, USA). The samples were incubated on ice for 10 minutes and centrifuged at 4 °C and 15800 g for 15 min. The supernatant was filtered using a 0.2 µm reversed cellulose membrane filter. Thus prepared metabolite extracts (10 µL) were injected directly for chromatographic separation on an ACQUITY UPLC BEH AMIDE column (1.7 µm, 2.1 × 150 mm, Waters) with a corresponding precolumn filter. After that, 400 µL of the metabolite extract were aliquoted and solvents were removed in

a vacuum dryer. The residual was resuspended in 75 mL of a mixture of water and methanol (95/5, v/v, both LC-MS grade, Fisher Scientific, Pittsburgh, USA), sonicated (10 min) and centrifuged (15 min, 15800 g) and transferred to LC vials with glass inserts for chromatographic separation on an ACQUITY UPLC BEH C18 column (1.7 μ m, 2.1 \times 150 mm, Waters). Also there, 10 μ L were injected for analysis. One sample per person was analyzed, analytical reproducibility was verified with quality control (QC) samples (pool of all samples). The samples were measured in batches of 60, with QC samples measured across each batch.

Chromatographic separation was performed on an ACQUITY UPLC system (I-Class, Waters, MA, USA). With the RP column, the flow rate was set to 240 μ L/min using a binary mixture of solvent A (water with 0.5 % methanol and 0.1 % formic acid) and solvent B (methanol with 0.1 % formic acid). The following gradient was used: 5 % B (1 min), 5 to 95 % B (9 min), 100 % B (2 min), and 5 % B (2 min). The column temperature was set to 30 $^{\circ}$ C and the autosampler was kept at 5 $^{\circ}$ C. For the AMIDE column a flow rate of 400 μ L/min was used with a binary mixture of solvent A (water with 0.1% formic acid) and solvent B (acetonitrile with 0.1% formic acid). The following gradient was applied: 99-30% B (7 min), 99% B (3 min). The column was kept at 45 $^{\circ}$ C and the autosampler at 5 $^{\circ}$ C.

Mass spectra were recorded on a quadrupole-time-of-flight high resolution mass spectrometer (TripleTOF 5600+, AB Sciex, Concord, ON, Canada) with a heated electrospray ionization source in positive and negative ion mode. Full-scan mass spectra (m/z range 50 to 650 Da) and data dependent MS-MS acquisitions (m/z range 40 to 650 Da) were performed. Curtain gas flow was set to 30 au, GS1 and GS2 were set to 60 au, a spray voltage of 5 kV (-4.5 kV) was applied and the ion source was heated to 500 $^{\circ}$ C. For the RP measurements, the total cycle time was kept at 800 ms to obtain at least 12 points/peak (minimal LC peak width = 9 s) with 150 ms for full scan MS and 85.7 ms for seven data dependent product ion scans acquired with a collision energy of 10/20/30 eV. For the AMIDE measurements, the total cycle time was kept at 550 ms to obtain at least 12 points/peak (minimal LC peak width = 6 s) with 150 ms for full scan MS and 87.5 ms for four data dependent product ion scans acquired with a collision energy of 10/20/30 eV.

Measurements of reference standards

In addition, reference standards were measured for a certain number of metabolites. Four different mixtures of non-isobaric compounds at a concentration of 10 μ g/mL, 5 μ g/mL and 1 μ g/mL in 5% methanol for RP measurements and 75% methanol for AMIDE measurements were produced (compositions of the four mixtures are given in Table S4). Moreover, 10 μ g/mL solutions were produced separately for linoleic acid, arachidonic acid, docosapenaenoic acid, myristic acid and ethanolamine. 10 μ L of each sample were injected for UPLC-MS measurements. Mass spectra were recorded in full scan and product ion mode. For measurements on the RP column, each acquisition cycle consisted of a full scan with an acquisition time of 150 ms and six product ion scans with an acquisition time of 100 ms. For measurements on the AMIDE column, each acquisition cycle consisted of a full scan with an acquisition time of 100 ms and four product ion scans with an

acquisition time of 100 ms. Collision energies are stated in Table S4, the other instrument parameters were set as described above for the data dependent acquisitions.

Data Preprocessing

Raw data files were converted into .mzXML files and centroided using MSConvert (ProteoWizard)²². Further preprocessing was conducted with XCMS^{23,24} in R (v3.6.1). For each measurement batch, peak picking, peak alignment, integration and annotation was performed. The applied parameter settings are given in Table S5.

Subsequently, data obtained from the QC samples was used to correct for instrumental drift using statTarget²⁵ in R. We applied the QCRLSC method (parameter settings: Frule = 0.8, QCspan = 0.5, degree = 2, imputeM = KNN) and removed all features that were detected in less than half of the QC samples as well as features, which had a relative standard deviation above 50% in the QCs after drift correction. Features identified as isotopes have also been removed. To confirm whether the drift correction did also remove inter-batch effects successfully, we compared the results of a principle component analysis before and after correction (Figure S8).

Finally, the features obtained from the different measurement batches were combined automatically (m/z tolerance: 0.001 Da, retention time tolerance: 15 s). This automatic merging failed for isomers with small differences in retention time, when large shifts in retention time occurred between batches. We therefore reviewed the merging by visual inspection of all extracted ion chromatograms and corrected manually for wrong assignments.

In addition to this untargeted peak extraction, we performed targeted analysis for metabolites, of which we measured reference standards. We used the peakPanther R package²⁶ with the target list given in Table S6. Retention time windows for isoleucine, pipecolinic acid, citric acid, 4-methyl-2-oxovaleric acid, phenyllactic acid, tetradecanedioic acid and docosapentaenoic acid were adapted for each batch, due to the presence of isomers at similar retention times. We applied drift correction with QC samples as described above.

Data from untargeted and targeted peak extraction were combined and only features detected in all samples were further considered. We removed features from the untargeted peak extraction approach, which were already covered by the targeted approach, in order to avoid duplicates. This resulted in 371 remaining features. Peak areas were log-transformed and autoscaled.

Metabolic pathway analysis and compound annotation

We made use of two different tools for automated compound annotation in order to annotate the peaks from our untargeted metabolic approach. We used MS Dial²⁷ for MS/MS library matching with the spectra we obtained from data dependent MS/MS acquisition. Moreover, we applied the mummichog algorithm²⁸ in MetaboAnalyst for R²⁹, which infers metabolic pathway information and biological activity. We employed the homo sapiens Kegg database, set the mass tolerance to 10 ppm and the p-value threshold to 0.2. We subsequently reviewed the annotations for biologically relevant features

manually and confirmed metabolite identities with reference standards, if available.

Statistical analysis

All data analyses were conducted in R (v3.6.1). In order to assess the correlation between the circadian period length measured in U2OS cells cultured in the presence of patient's serum and clinical parameters or metabolite levels in serum, we performed Kolmogorow-Smirnow (KS) tests between the first and the fourth data quartile. These comparisons were performed within the different patient groups (non-obese T2D, obese T2D, obese non-T2D, or control, or grouped as stated). Enrichment analysis of genome wide association study (GWAS) p-values against those of other traits was performed using gset package in R. Locuscompare package in R³⁰ was used to compare GWAS and eQTL signal at the *March1* locus. Coloc package in R was used to visualize GWAS and eQTL signals at the *March1* locus.

Genotyping

Fibroblasts were genotyped using the Illumina CoreExome 24 v1.3 array. Only samples with variant calling rate > 98 % were considered. Population stratification was done by principal component analysis using the phase 3 1000 genome variants to select for European subjects, resulting in 269 subjects qualified for genome wide association analyses (GWAS). Variants were then filtered to only choose those from the European panel. Next, variants were filtered using vcftools with the following parameters: --mac 2, --max-missing 0.95, --hwe 0.000001, yielding 290'867 genotyped variants. Genotyped variants were imputed using the Michigan Imputation Server with the phase 3 1000 genome genotypes as reference. Imputed variants were filtered out according to these criteria: imputation quality > 0.5, MAF > 0.05, Hardy-Weinberg probability < 1e-6. A total of 5'630'127 variants were left after filtering these steps.

Genome wide association analysis (GWAS)

GWAS was performed on circadian period length (inverse transformed using the following command line in R: `period length = qnorm((rank(x)-0.5)/length(x))`) using PLINK 1.90. Sex, age, disease (control, obese non T2D, non-obese T2D, and obese T2D), date of circadian measurement, experimenter, and the first 10 MDS dimensions of the genotypes were included as covariates.

External database

GWAS summary statistics for chronotypes or diabetes-related traits were downloaded from <http://www.nealelab.is/uk-biobank>, GWAS round 2. GWAS summary statistics for metabolites were taken from ³¹.

Results

Study design and patient cohort characteristics

Patients were recruited in the framework of the project dubbed Diachron that included non-obese T2D, obese T2D, obese non-T2D, and non-obese non-diabetic control subjects (see Materials and Methods for the study details). Patient characteristics and clinical parameters are summarized in Tables 1, S1-S3. Patients were genotyped to investigate genetic origin of individual differences in cellular oscillations. To study the effects of circulating factors on circadian traits in obesity and T2D, circadian rhythms of U2OS cells were continuously recorded in the presence of 10% serum from morning blood samples from the above-mentioned patients in the recording medium. For deep metabolic phenotyping, patients' sera were subjected to metabolomics analysis by liquid chromatography coupled to mass spectrometry (LC-MS) (see Figure 1A for the study design overview).

Circadian period length of U2OS cells assessed in the presence of obese patients' serum increases concomitant with severity of obesity

We observed huge inter-individual effects of sera on circadian period length measured in U2OS cells that varied between 20.69 h to 25.62 h across the entire cohort, with mean and standard deviation were 22.9 h and 0.8 h respectively (Figure 1B). The mean period length and standard deviation for each patient group were as following: control, 23.2 ± 0.7 h; obese non-T2D, 22.8 ± 0.8 h; non-obese T2D, 22.9 ± 0.7 h; and obese T2D, 23.0 ± 0.8 h. A one-way ANOVA revealed that there was a statistically significant difference in period length by patient group ($F(3)=4.308$, $p < 0.01$). A Tukey post-hoc test found that the mean value of period length was significantly different between obese non-T2D and control ($p < 0.01$, 95% C.I. = $[-0.68, -0.1]$), but not for any other pair-wise comparisons. Although statistical significance was observed, the huge inter-individual differences within each patient group and across the entire cohort suggests that such significance is of low biological relevance. It is more likely that inter-individual differences represent the main driver of the variation in circadian modifying effects of subjects' sera.

We next investigated the sources of inter-individual differences in serum factors that could explain the observed effects on circadian period length within each patient group. To this end, subjects were divided into quartiles based on various clinical parameters listed in Table 1, with the distribution of cellular period length from the first and the fourth quartile group compared to each other. For serum from T2D patients (non-obese T2D and obese T2D combined), such comparison yielded no statistically significant differences in the distribution of period length, except for triglycerides and ASAT (Figure S1A, $p < 0.05$ for triglycerides and ASAT, Kolmogorow-Smirnow test, not corrected for multiple testing). However, in the presence of sera from obese subjects (obese non-T2D and obese T2D combined), a period lengthening in U2OS cells was observed between quartiles separated based on increased HOMA-IR, insulin, HbA1c, fasting blood glucose, triglycerides, and decreased HDL (Figure 2, all $p < 0.05$, Kolmogorow-Smirnow test, not corrected for

multiple testing). Overall, deteriorated metabolic health in obese patients correlated with cellular period lengthening. For parameters that reflect liver and kidney function (ASAT and creatinine), a similar relationship was observed: worse liver and kidney function correlate with longer period length. Importantly, the same observation was not present for non-obese subjects (control and non-obese T2D combined) for these parameters (Figure S1B, all $p > 0.05$, Kolmogorow-Smirnow test, not corrected for multiple testing), nor for control subjects (Table S7, all $p > 0.05$, Kolmogorow-Smirnow test, not corrected for multiple testing). Overall, these observations suggest that severity of obesity is the most important aspect that correlates with differential effects of patients' sera on circadian period length.

Genome wide association analysis identified March1 as the gene most associated with period lengthening effects

Reasoning that individual differences in period lengthening by serum have genetic origin, we sought for genetic variants associated with period length measured in the presence of patient serum. Genome wide association analysis (GWAS) identified 613 variants that belong to 128 loci (Table S8, S9) associated with period length across the entire cohort. Interestingly, while the three top identified variants were intergenic, the fourth most associated variant (rs7654787) mapped to an intron of *March1* gene, known for its functions in antigen-presenting cells³² (Figure 3A, Figure S2). Noteworthy, *March1* knockout animals exacerbate obesity-induced insulin resistance stemming from its effects on CD8 T cell fate³³. In addition, *March1* knockout animals also exhibit enhanced insulin sensitivity and knockdown experiments shows that MARCH1 degrades surface insulin receptor in the basal state³⁴. The involvement of *March1* in insulin regulation prompted us to investigate the relationship between the identified *March1* variant and insulin resistance in our cohort. We observed that obese subjects carrying the homozygous AA allele had similar insulin and HOMA-IR compared to non-obese subjects (Figure 3B, 3C), in contrast to the expected higher insulin and HOMA-IR when being obese with other genotypes. This is also in line with allele A being associated with shorter period length (Figure 3A). The observed differences in insulin and HOMA-IR by AA genotype vs other genotypes of this MARCH1 variant were not observed when patients were stratified by T2D status (Figure S3). This is consistent with our former observation regarding the correlation of the metabolic status in obese patients with the period length in U2OS cells.

We next sought for evidence of activity at rs7654787 in publicly available data. We found that this variant is located within 2kb of cis regulatory elements (CRE, H3K4me3, H3K4me1, and H3K27Ac signatures) active in 7 cell lines in the ENCODE dataset (Figure S4A). In addition, expression quantitative trait loci (eQTL) analysis shows the correlation between genotypes and gene expression. We sought for published eQTLs in the pancreas³⁵ at rs7654787 and found suggestive evidence that rs6536810, which is in linkage disequilibrium with rs7654787 ($R^2=0.9956$), is associated with lower expression of *March1* ($p = 4e-07$, slope = -0.21, T statistic = -5.15, Figure S4B). In other words, combined with our data, allele A of *March1* variant is associated with lower expression of the gene, shorter period length,

and lower insulin and lower HOMA-IR. This observation is in line with the reported finding that MARCH1 expression increased in insulin-resistant vs insulin-sensitive subjects³⁴. This is also consistent with the results that *March1* knockdown and knockout mice showed improved glucose tolerance without an increase in insulin levels, suggesting enhanced insulin sensitivity in mice³⁴.

Identified GWAS variants are enriched in previously reported variants associated with extreme chronotype and T2D diabetes.

Since the here detected phenotype links circadian properties to diabetic status, we reason that there would be overlaps of our GWAS variants with those for chronotypes and diabetes-related traits. Indeed, our GWAS identified variants were enriched in those associated with Self-reported Chronotype and related traits, for instance variants linked to Sleep duration and Nap during the day in the UK Biobank database (Figure 4A). There was also enrichment for Diagnosed type 2 diabetes variants, but interestingly not for Self-reported type 2 diabetes variants. In addition, GWAS identified variants were enriched in Job involving night shift variants, as well as Depression, two traits that are often associated with T2D^{36,37}. Moreover, the beta coefficient of the association, which denote the directions of association, e.g. if a variant is associated with longer or shorter period length, called shortly here beta coefficient directions, were largely consistent between GWAS variants and trait variants (Figure 4B, 4C, and 4D). Variants that were associated with shorter period length were also associated with morningness, while variants that were associated with diabetic status were also associated with longer period. This is in agreement with our previous finding that *in vitro* circadian period length correlates with human chronotype²¹, and published work showing that late chronotype is associated with worse glycemic control^{38,39}.

Metabolomics reveals that circadian period lengthening is associated with insulin resistance in obese individuals

We observed that within the obese group, circadian period length did not correlate with BMI ($p = 0.43$, Kolmogorow-Smirnow test), indicating that obesity index alone cannot explain the period lengthening effects of sera from these subjects. It has been recognized that risk for cardiometabolic abnormalities varies among obese patients⁴⁰. In our Diachron cohort, we indeed observe such variation, with obese patients whose sera were classified in the first quartile in terms of triglycerides and fasting blood glucose and the fourth quartile of HDL cholesterol fitting the criteria for low cardiometabolic risk based on these parameters⁴¹ (Table S10, fasting serum triglycerides ≤ 1.7 mmol/l, fasting blood glucose ≤ 6.1 mmol/l, and HDL cholesterol serum concentrations > 1.0 mmol/l in men or > 1.3 mmol/l in women). This suggests that metabolic signature in the serum of obese patients affects circadian period length.

In order to obtain more detailed metabolic signature, we performed targeted and untargeted metabolomics of the patient sera by UPLC-MS. We detected

371 features in total, including 40 from targeted, and 331 from untargeted ones (Table S11, Table S12). Annotation of untargeted features by MS-DIAL²⁷ identified 78 of them (Table S13). We next analyzed the metabolic features in obese subjects (non-diabetic and diabetic combined) by quartiles based on each of detected metabolites. The cellular period length distribution measured in serum from the first and the fourth quartile group was compared. We observed a statistically significant shift in the distribution of period length between the first and fourth quartile for a range of compounds, including targeted and annotated untargeted ones (Figure 5A, 5B). For most of the compounds, the distribution of period length shifted toward longer values with higher levels of compounds, with few compounds only exhibiting the opposite tendency (one of lysophosphatidylcholine species, succinic acid, and serotonin, see Discussion). In addition to annotation of untargeted feature, we also employed the mummichog algorithm to infer pathway activity without feature identification to gain information from the whole untargeted metabolites²⁸. Metabolic pathway enrichment analysis on all untargeted features suggested that branched-chain amino acid (BCAA) degradation and biosynthesis were as among the most involved metabolic pathways (Table S14). It has been reported that circulating BCAAs are elevated in subjects with insulin resistance and T2D⁴². Concordantly, we observe that many of the metabolites associated with period length were also associated with insulin resistance score (HOMA-IR) in our cohort (Figure S5).

In addition, we explored the association between serum lipid landscape and cellular period length, based on the serum lipidomics analyses on the sub-set of this cohort that we have recently reported (see Table S15)⁴³. We detected statistically significant association between longer cellular period and lower levels of phospholipids, specifically LysoPE, PC, and LysoPC species (Figure 5C). This finding is consistent with the earlier observation that lower levels of phospholipids are associated with insulin resistance^{44,45}. Overall, we report that serum metabolic status associated with insulin resistance in obese patients may account for the period lengthening effect in U2OS cells.

GWAS variants are enriched in branched-chain amino acid variants

If serum metabolite levels are associated with serum's effects on period length that are partially explained by genetic variants, there should be overlaps between our GWAS variants and those explaining metabolite levels. Indeed, we found that GWAS variants are enriched in branched-chain amino acid (BCAA) and branched-chain keto acid (BCKA) variants (Figure S6A). Comparison of beta coefficient direction between GWAS variants and the metabolite variants confirmed that longer period measured in U2OS cells is associated with higher levels for all BCAAs and BCKAs in the patients' sera (Figure S6B).

Discussion

Obesity is often accompanied by metabolic syndrome as a comorbidity⁴⁶, characterized by abdominal obesity, high blood pressure, high blood sugar and triglyceride levels, low HDL cholesterol, and insulin resistance⁴⁷. Our

study suggests that alterations in serum featuring metabolic syndrome of obese patients have period lengthening effect on U2OS cellular oscillations, in line with longer period observed in mice with high-fat diet induced obesity⁷. Notably, we did not find a correlation between period length and BMI, suggesting that it is not weight gain *per se*, but rather metabolic signature alterations associated with metabolic syndrome are responsible for the changes in circadian characteristics observed in cultured cells.

Taking a multi-omic approach, we mapped insulin resistance as the parameter that is associated with a circadian period modifying effect. Our genetic analysis using cellular phenotype linked MARCH1, whose regulatory role in insulin resistance development have been demonstrated previously^{33,34,48}, to changes in cellular circadian period length exerted by individual differences in serum components. Indeed, higher MARCH1 expression was reported in white adipose tissue from obese insulin-resistant subjects³⁴. Interestingly, the variant in *March1* gene, rs7654787, seems to have a protective effect since it is associated with shorter period length, and lower MARCH1 expression. Meta-analysis of phenome-wide association (PheWAS) confirms that this variant is negatively correlated with BMI (Figure S7). The second PheWAS phenotype is Platelet count, for which a closer look at our data revealed that in fact in obese subjects, shorter period length was also associated with lower platelet count ($p = 0.004$, Kolmogorow-Smirnow test), consistent with the negative beta coefficient. Platelet count has been shown to be higher in impaired fasting glucose and metabolic syndrome (but not T2D), and is associated with insulin resistance^{49,50}. Thus, our genetic approach using cellular phenotype allow to identify not only the circulating factors that affect circadian traits, but also pinpointed the hematological phenotype that we were not aware of in the first place.

Our metabolomic and lipidomic profiling further identify a panel of insulin resistance-related metabolites and lipids interacting with the circadian clock. In addition to the well-described branched chain amino acids and branched chain keto acids, we also found a positive correlation between glutamic acid levels in serum and insulin resistance, corroborating results reported in the literature⁵¹. A correlation between uridine levels in urine and HOMA-IR have been observed in humans before⁵² and injection of uridine in obese mice induced deterioration of glucose tolerance⁵³. Also, upregulation of the kynurenine pathway has been related to insulin resistance in obesity. Tryptophan can be metabolized either to kynurenine or to serotonin. It has been suggested that inflammation in obesity induces upregulation of the tryptophan-kynurenine route⁵⁴. Activation of this pathway results in increased levels of xanthurenic acid, which can form complexes with insulin that are less active than insulin itself⁵⁵. In line with these findings, serotonin was reported to enhance insulin secretion⁵⁵ and we observed an inverse relation between serotonin levels in serum and circadian period length. Similarly, for succinic acid⁵⁶, and lysophosphatidylcholine⁵⁷ enhancing effects on insulin release have been reported. We found for increased serum levels of these metabolites a shortening of the circadian period length. This further indicates insulin resistance being a key factor in the alteration of circadian clock properties.

Insulin has been shown to lengthen period length in mouse cells by increasing PER2 protein synthesis via simultaneous mTOR activation and miRNA-mediated posttranscriptional regulation⁵⁸. Thus, higher serum insulin in obese subjects likely prolongs period length of cellular oscillations in U2OS cells in a similar way. Secondly, metabolic pathway analysis indicated disturbed BCAA metabolism to be the most enriched pathway contributing to period lengthening. Within the last decade, evidence for the association between increased circulating BCAAs and insulin resistance has emerged⁴². Animal models have suggested, that elevated BCAA levels lead to hyperactivation of mTORC1 followed by activation of the ribosomal kinase S6K1. This leads to phosphorylation and thereby inhibition of insulin receptor substrate 1 (IRS-1) resulting in insulin resistance⁵⁹. Although it is still under investigation if the same mechanism underlies insulin resistance in obese individuals, activation of the mTOR pathway by BCAA is one possible way that these circulating amino acids contribute to circadian period lengthening. Of note, as Crosby *et al.* has shown, mTOR activation alone is not sufficient to induce PER2 translation, but synergic mTOR activation and inhibition of PER2-regulating miRNAs by insulin is required for increase in PER2 translation that leads to period lengthening⁵⁸. This could explain the discrepancy in period modifying effects of mTOR activation in flies and in mice. In *Drosophila*, Seghal and co-workers found circadian period lengthening upon mTORC1 activation⁶⁰. However, in mice, Ramanathan *et al.* reported that mTOR activation shortened period length, with the protein levels of CLOCK, BMAL1, and CRY1 but not PERs being affected⁶¹. Therefore, the effect of mTOR activation on the circadian clocks is likely context dependent. Alternatively, BCAA, especially leucine and ketoleucine, as potent insulin secretagogues^{62,63}, may exert their effects on circadian period length indirectly, mediated via insulin. Unraveling potential mechanisms underlying the reported here intricate link between insulin resistance and altered cellular circadian rhythms warrants further studies.

Collectively, our multi-omics analyses identify circulating metabolic factors characteristic of insulin resistance that affect cellular circadian properties. Moreover, we provide novel clues on how shared genomic and metabolomic factors related to obesity and T2D affect cellular circadian traits that could be measured in a commonly used U2OS cell line.

References

1. Poggiogalle, E., Jamshed, H. & Peterson, C. M. Circadian regulation of glucose, lipid, and energy metabolism in humans. *Metabolism*. **84**, 11–27 (2018).
2. Piorz, V., Helfrich-Förster, C. & Oster, H. The role of the circadian clock system in physiology. *Pflugers Arch. Eur. J. Physiol.* **470**, 227–239 (2018).
3. Sinturel, F., Petrenko, V. & Dibner, C. Circadian Clocks Make Metabolism Run. *J. Mol. Biol.* **432**, 3680–3699 (2020).
4. Yoon, J.-A. *et al.* Meal time shift disturbs circadian rhythmicity along with metabolic and behavioral alterations in mice. *PLoS One* **7**, e44053

- 647 (2012).
- 648 5. Garaulet, M. & Gómez-Abellán, P. Timing of food intake and obesity: a
649 novel association. *Physiol. Behav.* **134**, 44–50 (2014).
- 650 6. Mukherji, A., Kobiita, A. & Chambon, P. Shifting the feeding of mice to
651 the rest phase creates metabolic alterations, which, on their own, shift
652 the peripheral circadian clocks by 12 hours. *Proc. Natl. Acad. Sci.*
653 1519735112- (2015) doi:10.1073/pnas.1519735112.
- 654 7. Kohsaka, A. *et al.* High-Fat Diet Disrupts Behavioral and Molecular
655 Circadian Rhythms in Mice. *Cell Metab.* **6**, 414–421 (2007).
- 656 8. Oishi, K. & Higo-Yamamoto, S. Disrupted daily light-dark cycles induce
657 physical inactivity and enhance weight gain in mice depending on
658 dietary fat intake. *Neuroreport* **25**, 865–869 (2014).
- 659 9. Kim, S. M. *et al.* Shift work cycle-induced alterations of circadian
660 rhythms potentiate the effects of high-fat diet on inflammation and
661 metabolism. *FASEB J.* **32**, 3085–3095 (2018).
- 662 10. Petrenko, V. *et al.* In pancreatic islets from type 2 diabetes patients, the
663 dampened circadian oscillators lead to reduced insulin and glucagon
664 exocytosis. *Proc. Natl. Acad. Sci. U. S. A.* **117**, 2484–2495 (2020).
- 665 11. Gubin, D. G. *et al.* Disrupted circadian rhythms of body temperature,
666 heart rate and fasting blood glucose in prediabetes and type 2 diabetes
667 mellitus. *Chronobiol. Int.* **34**, 1136–1148 (2017).
- 668 12. Reutrakul, S. & Knutson, K. L. Consequences of Circadian Disruption
669 on Cardiometabolic Health. *Sleep Med. Clin.* **10**, 455–468 (2015).
- 670 13. Mason, I. C., Qian, J., Adler, G. K. & Scheer, F. A. J. L. Impact of
671 circadian disruption on glucose metabolism: implications for type 2
672 diabetes. *Diabetologia* **63**, 462–472 (2020).
- 673 14. Association, A. D. 2. Classification and Diagnosis of Diabetes:
674 Standards of Medical Care in Diabetes—2021. *Diabetes Care* **44**, S15–
675 S33 (2020).
- 676 15. Kane, J. P., Pullinger, C. R., Goldfine, I. D. & Malloy, M. J. Dyslipidemia
677 and diabetes mellitus: Role of lipoprotein species and interrelated
678 pathways of lipid metabolism in diabetes mellitus. *Curr. Opin.*
679 *Pharmacol.* **61**, 21–27 (2021).
- 680 16. Chen, Z. Z. & Gerszten, R. E. Metabolomics and Proteomics in Type 2
681 Diabetes. *Circ. Res.* 1613–1627 (2020)
682 doi:10.1161/CIRCRESAHA.120.315898.
- 683 17. White, P. J. *et al.* Insulin action, type 2 diabetes, and branched-chain
684 amino acids: A two-way street. *Mol. Metab.* **52**, 101261 (2021).
- 685 18. Pagani, L. *et al.* Serum factors in older individuals change cellular clock
686 properties. *Proc. Natl. Acad. Sci. U. S. A.* **108**, 7218–7223 (2011).
- 687 19. Sinturel, F. *et al.* Cellular circadian period length inversely correlates
688 with HbA1c levels in individuals with type 2 diabetes. *Diabetologia* **62**,
689 1453–1462 (2019).

- 690 20. Du, N.-H. & Brown, S. A. Measuring Circadian Rhythms in Human Cells
691 BT - Circadian Clocks: Methods and Protocols. in (ed. Brown, S. A.)
692 53–67 (Springer US, 2021). doi:10.1007/978-1-0716-0381-9_4.
- 693 21. Brown, S. A. *et al.* The period length of fibroblast circadian gene
694 expression varies widely among human individuals. *PLoS Biol.* **3**, e338
695 (2005).
- 696 22. Kessner, D., Chambers, M., Burke, R., Agus, D. & Mallick, P.
697 ProteoWizard: open source software for rapid proteomics tools
698 development. *Bioinformatics* **24**, 2534–2536 (2008).
- 699 23. Smith, C. A., Want, E. J., O'Maille, G., Abagyan, R. & Siuzdak, G.
700 XCMS: Processing Mass Spectrometry Data for Metabolite Profiling
701 Using Nonlinear Peak Alignment, Matching, and Identification. *Anal.*
702 *Chem.* **78**, 779–787 (2006).
- 703 24. Tautenhahn, R., Böttcher, C. & Neumann, S. Highly sensitive feature
704 detection for high resolution LC/MS. *BMC Bioinformatics* **9**, 504 (2008).
- 705 25. Luan, H., Ji, F., Chen, Y. & Cai, Z. statTarget: A streamlined tool for
706 signal drift correction and interpretations of quantitative mass
707 spectrometry-based omics data. *Anal. Chim. Acta* **1036**, 66–72 (2018).
- 708 26. Wolfer, A. M. *et al.* peakPantheR, an R package for large-scale targeted
709 extraction and integration of annotated metabolic features in LC–MS
710 profiling datasets. *Bioinformatics* **37**, 4886–4888 (2021).
- 711 27. Tsugawa, H. *et al.* MS-DIAL: data-independent MS/MS deconvolution
712 for comprehensive metabolome analysis. *Nat. Methods* **12**, 523–526
713 (2015).
- 714 28. Li, S. *et al.* Predicting Network Activity from High Throughput
715 Metabolomics. *PLoS Comput. Biol.* **9**, (2013).
- 716 29. Chong, J., Wishart, D. S. & Xia, J. Using MetaboAnalyst 4.0 for
717 Comprehensive and Integrative Metabolomics Data Analysis. *Curr.*
718 *Protoc. Bioinforma.* **68**, e86 (2019).
- 719 30. Liu, B., Gloudemans, M. J., Rao, A. S., Ingelsson, E. & Montgomery, S.
720 B. Abundant associations with gene expression complicate GWAS
721 follow-up. *Nat. Genet.* **51**, 768–769 (2019).
- 722 31. Shin, S.-Y. *et al.* An atlas of genetic influences on human blood
723 metabolites. *Nat. Genet.* **46**, 543–550 (2014).
- 724 32. Liu, H., Minter, J. D. & Villadangos, J. A. MARCH ligases in immunity.
725 *Curr. Opin. Immunol.* **58**, 38–43 (2019).
- 726 33. Majdoubi, A. *et al.* Lack of the E3 Ubiquitin Ligase March1 Affects CD8
727 T Cell Fate and Exacerbates Insulin Resistance in Obese Mice. *Front.*
728 *Immunol.* **11**, 1–14 (2020).
- 729 34. Nagarajan, A. *et al.* MARCH1 regulates insulin sensitivity by controlling
730 cell surface insulin receptor levels. *Nat. Commun.* **7**, (2016).
- 731 35. Viñuela, A. *et al.* Genetic variant effects on gene expression in human
732 pancreatic islets and their implications for T2D. *Nat. Commun.* **11**,
733 (2020).

- 734 36. Strohmaier, S., Devore, E. E., Zhang, Y. & Schernhammer, E. S. A
735 Review of Data of Findings on Night Shift Work and the Development of
736 DM and CVD Events: a Synthesis of the Proposed Molecular
737 Mechanisms. *Curr. Diab. Rep.* **18**, (2018).
- 738 37. Holt, R. I. G., De Groot, M. & Golden, S. H. Diabetes and depression.
739 *Curr. Diab. Rep.* **14**, (2014).
- 740 38. Iwasaki, M. *et al.* Morningness-eveningness questionnaire score
741 correlates with glycated hemoglobin in middle-aged male workers with
742 type 2 diabetes mellitus. *J. Diabetes Investig.* **4**, 376–381 (2013).
- 743 39. Reutrakul, S. *et al.* Chronotype is independently associated with
744 glycemic control in type 2 diabetes. *Diabetes Care* **36**, 2523–2529
745 (2013).
- 746 40. Iacobini, C., Pugliese, G., Blasetti Fantauzzi, C., Federici, M. & Menini,
747 S. Metabolically healthy versus metabolically unhealthy obesity.
748 *Metabolism.* **92**, 51–60 (2019).
- 749 41. Tsatsoulis, A. & Paschou, S. A. Metabolically Healthy Obesity: Criteria,
750 Epidemiology, Controversies, and Consequences. *Curr. Obes. Rep.* **9**,
751 109–120 (2020).
- 752 42. Lynch, C. J. & Adams, S. H. Branched-chain amino acids in metabolic
753 signalling and insulin resistance. *Nat. Rev. Endocrinol.* **10**, 723–736
754 (2014).
- 755 43. Sinturel, F. *et al.* Circadian organization of lipid landscape is perturbed
756 in type 2 diabetic patients. *Cell Reports Med.* **4**, 101299 (2023).
- 757 44. Tonks, K. T. *et al.* Skeletal muscle and plasma lipidomic signatures of
758 insulin resistance and overweight/obesity in humans. *Obesity* **24**, 908–
759 916 (2016).
- 760 45. Yin, X. *et al.* Lipidomic profiling identifies signatures of metabolic risk.
761 *EBioMedicine* **51**, (2020).
- 762 46. Mongraw-Chaffin, M. *et al.* Metabolically Healthy Obesity, Transition to
763 Metabolic Syndrome, and Cardiovascular Risk. *J. Am. Coll. Cardiol.* **71**,
764 1857–1865 (2018).
- 765 47. McCracken, E., Monaghan, M. & Sreenivasan, S. Pathophysiology of
766 the metabolic syndrome. *Clin. Dermatol.* **36**, 14–20 (2018).
- 767 48. Bhagwandin, C. *et al.* The E3 ubiquitin ligase MARCH1 regulates
768 glucose-tolerance and lipid storage in a sex-specific manner. *PLoS One*
769 **13**, 1–14 (2018).
- 770 49. Balducci, Stefano, Sacchetti, Massimo, Haxhi, Jonida, Orlando, Giorgio,
771 D'Errico, Valeria, Fallucca, Sara, Menini, Stefano, Pugliese, G. Platelet
772 mean volume, distribution width, and count in type 2 diabetes, impaired
773 fasting glucose, and metabolic syndrome: a meta-analysis. *Diabetes.*
774 *Metab. Res. Rev.* **32**, 13–23 (2014).
- 775 50. Taniguchi, A. *et al.* Platelet count is independently associated with
776 insulin resistance in non-obese Japanese type 2 diabetic patients.
777 *Metabolism.* **52**, 1246–1249 (2003).

51. Seibert, R. *et al.* Relationship between insulin resistance and amino acids in women and men. *Physiol. Rep.* **3**, 1–7 (2015).
52. Zhang, Y., Guo, S., Xie, C. & Fang, J. Uridine Metabolism and Its Role in Glucose, Lipid, and Amino Acid Homeostasis. *Biomed Res. Int.* **2020**, 1–7 (2020).
53. Deng, Y. *et al.* An adipo-biliary-uridine axis that regulates energy homeostasis. *Science (80-.).* **355**, (2017).
54. Favennec, M. *et al.* The kynurenine pathway is activated in human obesity and shifted toward kynurenine monooxygenase activation. *Obesity* **23**, 2066–2074 (2015).
55. Oxenkrug, G. Insulin resistance and dysregulation of tryptophan-kynurenine and kynurenine-nicotinamide adenine dinucleotide metabolic pathways. *Mol. Neurobiol.* **48**, 294–301 (2013).
56. Alarcon, C., Wicksteed, B., Prentki, M., Corkey, B. E. & Rhodes, C. J. Succinate is a preferential metabolic stimulus-coupling signal for glucose-induced proinsulin biosynthesis translation. *Diabetes* **51**, 2496–2504 (2002).
57. Drzazga, A. *et al.* Lysophosphatidylcholine and its phosphorothioate analogues potentiate insulin secretion via GPR40 (FFAR1), GPR55 and GPR119 receptors in a different manner. *Mol. Cell. Endocrinol.* **472**, 117–125 (2018).
58. Crosby, P. *et al.* Insulin/IGF-1 Drives PERIOD Synthesis to Entrain Circadian Rhythms with Feeding Time. *Cell* **177**, 896–909.e20 (2019).
59. Newgard, C. B. *et al.* A Branched-Chain Amino Acid-Related Metabolic Signature that Differentiates Obese and Lean Humans and Contributes to Insulin Resistance. *Cell Metab.* **9**, 311–326 (2009).
60. Zheng, X. & Sehgal, A. AKT and TOR signaling set the pace of the circadian pacemaker. *Curr. Biol.* **20**, 1203–1208 (2010).
61. Ramanathan, C. *et al.* mTOR signaling regulates central and peripheral circadian clock function. *PLoS Genet.* **14**, 1–21 (2018).
62. Neinast, M., Murashige, D. & Arany, Z. Branched Chain Amino Acids. *Annu. Rev. Physiol.* **81**, 139–164 (2019).
63. Arany, Z. & Neinast, M. Branched Chain Amino Acids in Metabolic Disease. *Curr. Diab. Rep.* **18**, 1–8 (2018).

Figure legends:

Figure 1: Individual sera have profound effects on circadian period length of U2OS cell oscillations. (A) Study design: type 2 diabetes (T2D, subdivided into non-obese and obese) subjects, obese non-T2D subjects and control subjects were recruited. Cell culture medium containing 10% serum from each subject was incubated on U2OS cells to measure changes in circadian parameters exerted by circulating components. Basic blood chemistry test, patient genotyping, as well as, metabolite profiling by LC-MS were performed to identify genetic and metabolomic factors affecting circadian traits. (B)

822 Circadian period length measured in U2OS cells in the presence of patient's
823 serum.

824 Figure 2: Clinical parameters related to severity of obesity in the group of
825 obese subjects (obese non-T2D and obese T2D combined) were associated
826 with longer cellular period length. For each blood parameter, patients were
827 divided into quartiles for that parameter. Period lengths were then compared
828 between the 1st and the 4th quartile. Shown are blood parameters that have
829 statistically significant difference between these two quartiles ($p < 0.05$,
830 Kolmogorov-Smirnov test, one-sided).

831 Figure 3: A variant in the intron of *March1* gene is associated with period
832 length and has an impact on insulin and HOMA-IR levels. (A) The A allele of
833 variant rs7654787 is associated with shorter period length in U2OS cells. (B)
834 Insulin level stratified by genotype of variant rs7654787 and obese state. (C)
835 HOMA-IR stratified by genotype of variant rs7654787 and obese state. ***: p
836 < 0.0001 , **: $p < 0.001$, *: $p < 0.01$, ns: not significant, Tukey's range test.

837 Figure 4: GWAS variants are enriched in chronotype and diabetes-related
838 traits in UKBiobank. (A) Enrichment analysis was done for p-values of the
839 613 GWAS variants against those of all variants in the listed traits. Shown is
840 the p-value of the enrichment analysis for each trait. Red line indicates $p =$
841 0.05 . (B) Beta coefficient directions between period length and traits that had
842 a p-value < 0.05 in (A) were compared. Shown are p-value of chi-squared
843 test of dependency. Red line indicates $p = 0.05$. (C) and (D) Examples of
844 beta coefficient directions between period length and traits. (C) Variants that
845 are associated with shorter period length are associated with a morningness
846 phenotype. (D) Variants that are associated with longer period length are
847 associated with higher T2D risk.

848 Figure 5: Metabolites and lipids associated with insulin resistance are
849 associated with longer period length in U2OS cells. (A) Metabolite levels
850 associated with period length in obese subjects are shown. They are sorted
851 by p-value, and direction of comparison with period length (longer period
852 length indicated by positive values). Red lines indicate $p = 0.05$ (one-sided
853 Kolmogorov-Smirnov test comparing the 1st vs the 4th quartile as in Figure 2)
854 for each direction. (B) Examples of cumulative distribution comparing period
855 length between patients falling in the 1st vs the 4th quartile for each
856 metabolite. (C) Correlation between phospholipid levels and period length in
857 obese subjects. LysoPE: Spearman correlation coefficient = -0.45 , $p = 0.01$.
858 PC: $\text{cor} = -0.36$, $p = 0.04$. LysoPC: $\text{cor} = -0.37$, $p = 0.04$.

859 Figure S1: Association between clinical parameters and circadian period
860 length in obese participants, but not other groups. (A) Clinical parameters for
861 T2D subjects (non-obese T2D and obese T2D combined). Only Triglycerides
862 and ASAT showed statistically significant differences ($p < 0.05$, Kolmogorov-
863 Smirnov test, one-sided). (B) Clinical parameters for non-obese subjects
864 (controls and non-obese T2D combined).

865 Figure S2: Genome-wide association study (GWAS) identified variants that
866 are associated with circadian period length measured in U2OS cells. (A)
867 Manhattan plot showed the top variants associated with period length. While
868 the top three variants are intergenic, the 4th variant mapped to the intron of

869 *March1* gene (marked by an arrow). (B) Q-Q plot showing the expected vs.
870 observed GWAS p-values.

871 Figure S3: Genotype at rs7654787 did not influence insulin and HOMA-IR
872 levels when stratifying patients by T2D status. (A) Insulin level stratified by
873 genotype of variant rs7654787 and T2D status. (B) HOMA-IR stratified by
874 genotype of variant rs7654787 and T2D status. ***: $p < 0.0001$, **: $p < 0.001$,
875 *: $p < 0.01$, ns: not significant, Tukey's range test.

876 Figure S4: Confirmation that rs7654787 is active. (A) Genome Browser view
877 showing variant rs7654787 (whose position marked by a blue vertical line) is
878 located near *cis* regulatory region (CRE, H3K4me3, H3K3me1, and H3K27Ac
879 signatures). (B) Variant rs6536810, which is in linkage disequilibrium with
880 rs7654787 ($R^2=0.9956$), is colocalised with expression quantitative trait loci
881 (eQTL) signals in the pancreas. Left panel compared eQTL vs GWAS p-value
882 for variant rs6536810. Right panels show GWAS (upper) and eQTL (lower) p-
883 values for variants around the colocalisation coordinate. Plot was produced
884 using coloc R package.

885 Figure S5: Targeted and untargeted metabolites that are associated with
886 HOMA-IR. ***: $p < 0.001$, **: $p < 0.01$, * $p < 0.05$. HOMA-IR between obese
887 subjects that fall in the 1st vs the 4th quartile for each metabolite.

888 Figure S6: GWAS variants are enriched in metabolite variants. (A) p-values
889 of enrichment analysis. (B) Examples of beta coefficient direction.

890 Figure S7: PheWAS of variant rs7654787 (image represents screen shot from
891 hugeamp.org, or Common Metabolic Diseases Knowledge Portal).

892 Figure S8: Principal component analysis before (a) and after (b) instrumental
893 drift correction.

894

895 **Table titles**

896 Table 1: Characteristics of the study groups. Footnote: ¹ Median (IQR), n (%);
897 ² Kruskal-Wallis rank sum test, Pearson's Chi-squared test.

898 Table S1: Patient inclusion criteria.

899 Table S2: Patient exclusion criteria.

900 Table S3: Serum clinical parameters of subjects.

901 Table S4: Composition of standard mixtures of reference compounds and
902 collision energies used for the acquisition of product ion scans.

903 Table S5: Parameter settings for preprocessing of LC-MS data using XCMS in
904 R.

905 Table S6: Target list for targeted peak extraction.

906 Table S7: P-values of Kolmogorov-Smirnov test comparing the period length
907 between the first and the fourth quartile for control subjects.

908 Table S8: List of the GWAS variants and their associated p-values.

909 Table S9: List of clumped GWAS variants based on empirical estimates of
910 linkage disequilibrium between SNPs.

911 Table S10: Quartiles of serum clinical parameters for obese subjects.

912 Table S11: ID of targeted metabolites.

913 Table S12: Metabolite levels for all subjects.

914 Table S13: Targeted and untargeted metabolites information and their
915 annotation.

916 Table S14: Metabolite pathway enrichment in obese subjects.

917 Table S15: Lipidomics of a subset of subjects.

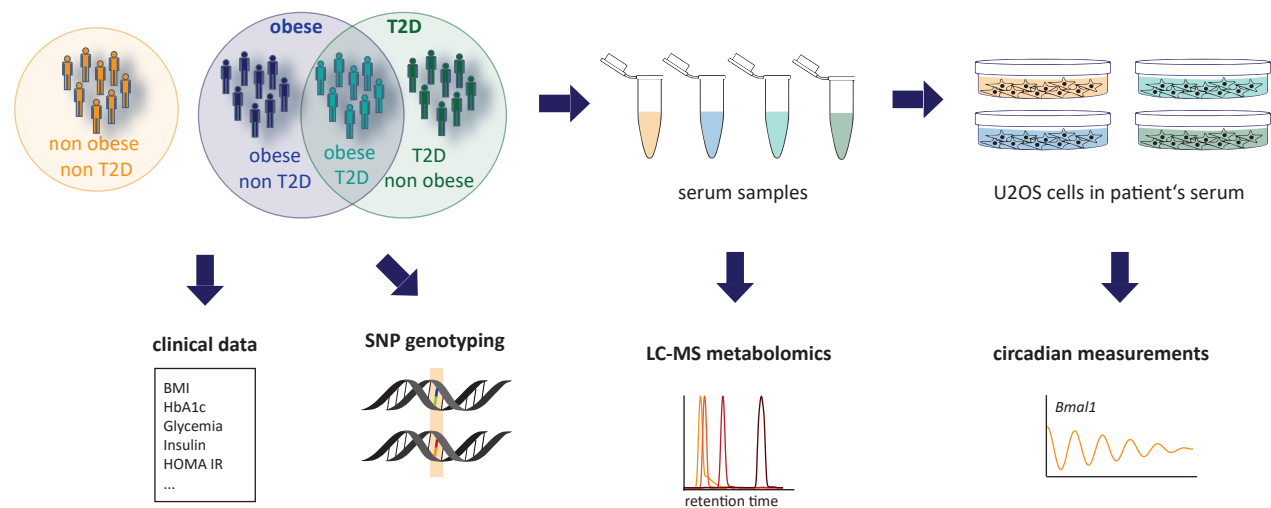
Table 1. Characteristics of the study groups

Characteristic	Control, N = 97 ¹	Obese non T2D, N = 85 ¹	Non obese T2D, N = 52 ¹	Obese T2D, N = 40 ¹	p-value ²
Age (years)	57 (51, 64)	52 (48, 61)	64 (57, 67)	64 (55, 70)	<0.001
Sex					0.019
Female	56 (58%)	40 (47%)	18 (35%)	14 (35%)	
Male	41 (42%)	45 (53%)	34 (65%)	26 (65%)	
BMI (kg/m ²)	24.3 (20.5, 27.3)	33.4 (31.4, 35.7)	26.1 (23.4, 28.2)	34.2 (32.5, 36.5)	<0.001
HbA1c (%)	5.30 (5.10, 5.40)	5.40 (5.30, 5.60)	7.00 (6.68, 7.80)	7.65 (7.10, 8.53)	<0.001
Fasting blood glucose (mmol/l)	5.10 (4.90, 5.40)	5.40 (5.10, 5.90)	7.95 (7.07, 9.10)	9.10 (7.77, 11.17)	<0.001
Insulin (mU/l)	7 (5, 9)	14 (10, 21)	10 (7, 13)	21 (12, 28)	<0.001
HOMA-IR	1.5 (1.1, 2.2)	3.6 (2.4, 5.3)	3.5 (2.4, 4.9)	7.9 (4.8, 12.7)	<0.001
Total cholesterol (mmol/l)	5.30 (4.70, 6.00)	5.30 (4.70, 5.90)	4.90 (3.70, 5.60)	5.00 (4.27, 5.60)	0.004
HDL-cholesterol (mmol/l)	1.72 (1.47, 2.08)	1.30 (1.11, 1.47)	1.23 (1.04, 1.46)	1.15 (0.98, 1.48)	<0.001
LDL-cholesterol (mmol/l)	2.86 (2.34, 3.65)	3.19 (2.53, 3.75)	2.45 (1.71, 3.35)	2.51 (1.77, 3.19)	<0.001
Triglyceride (mmol/l)	1.01 (0.79, 1.30)	1.36 (1.09, 1.89)	1.45 (1.06, 2.55)	1.81 (1.26, 2.78)	<0.001
Leptin (ng/ml)	5 (3, 12)	23 (10, 40)	7 (4, 11)	23 (14, 28)	<0.001
Cortisol (nmol/l)	389 (315, 457)	312 (254, 410)	360 (288, 466)	390 (274, 462)	0.003
TSH (mU/l)	2.07 (1.62, 2.83)	2.15 (1.47, 2.91)	1.97 (1.52, 2.90)	2.04 (1.65, 3.17)	>0.9
Urea (mmol/l)	4.70 (4.10, 5.90)	5.30 (4.40, 6.30)	5.60 (4.77, 7.50)	5.45 (4.97, 6.90)	<0.001
Creatinine (μmol/l)	77 (65, 86)	77 (67, 89)	80 (67, 92)	82 (67, 91)	0.5
ALAT (U/l)	21 (18, 29)	27 (21, 37)	28 (22, 33)	42 (26, 65)	<0.001
ASAT (U/l)	23 (19, 27)	24 (19, 29)	22 (19, 29)	30 (22, 36)	0.034
GGT (U/l)	21 (15, 31)	25 (18, 50)	28 (20, 43)	50 (30, 89)	<0.001
Alkaline phosphatase (U/l)	62 (52, 77)	67 (57, 77)	61 (51, 74)	76 (59, 95)	0.027
Total bilirubin (μmol/l)	10 (8, 15)	8 (7, 12)	9 (7, 12)	8 (7, 10)	0.012
Heart beat	66 (60, 73)	70 (62, 79)	72 (65, 80)	78 (70, 84)	<0.001
Systolic blood pressure (mm Hg)	118 (107, 131)	131 (119, 134)	130 (119, 141)	133 (128, 138)	<0.001
Diastolic blood pressure (mm Hg)	72 (66, 79)	78 (70, 86)	76 (70, 81)	79 (73, 83)	<0.001

¹ Median (IQR); n (%)² Kruskal-Wallis rank sum test; Pearson's Chi-squared test

Figure 1

A



B

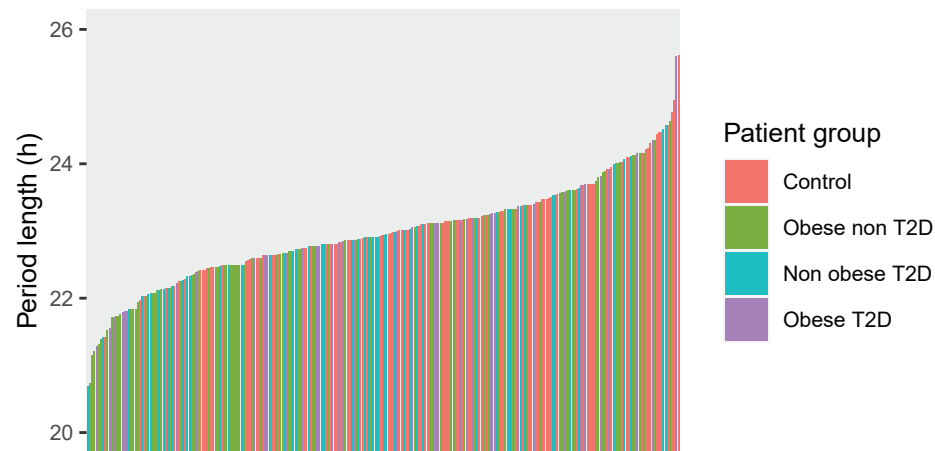


Figure 2

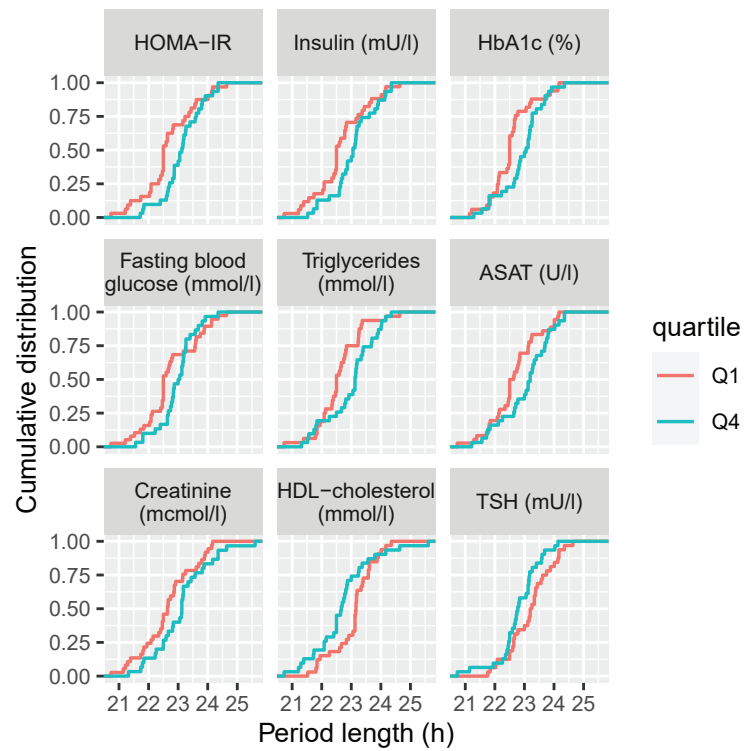
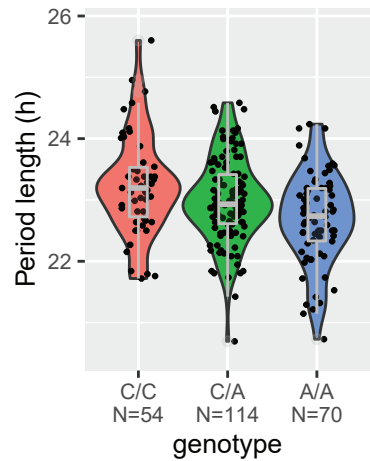
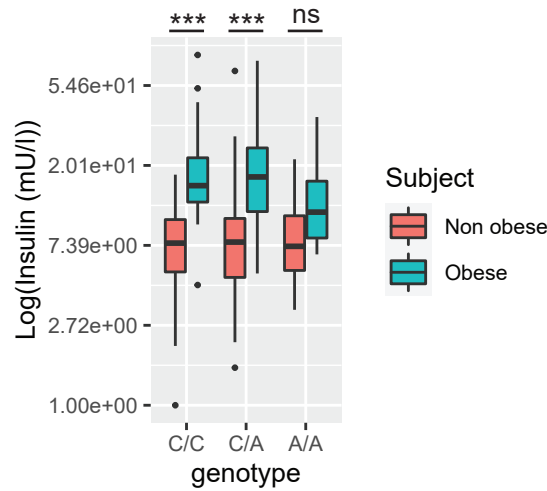


Figure 3

A



B



C

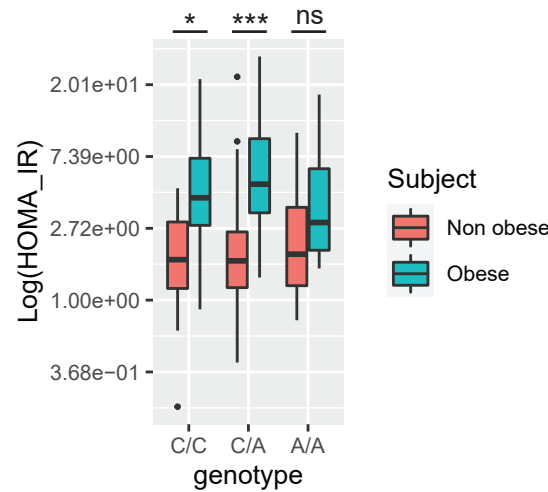
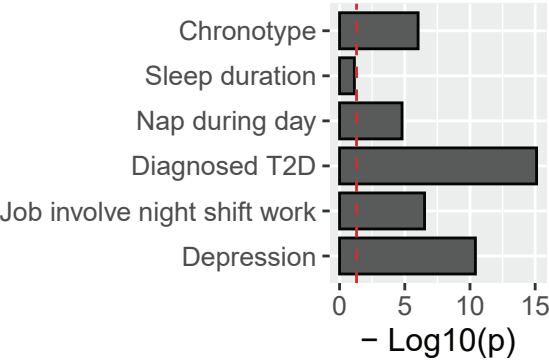


Figure 4

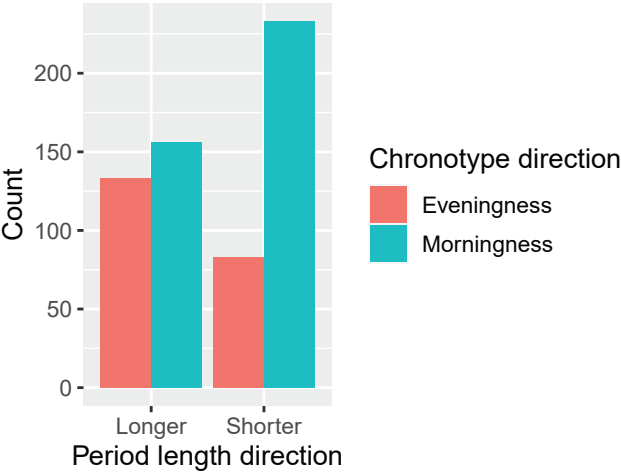
A



B



C



D

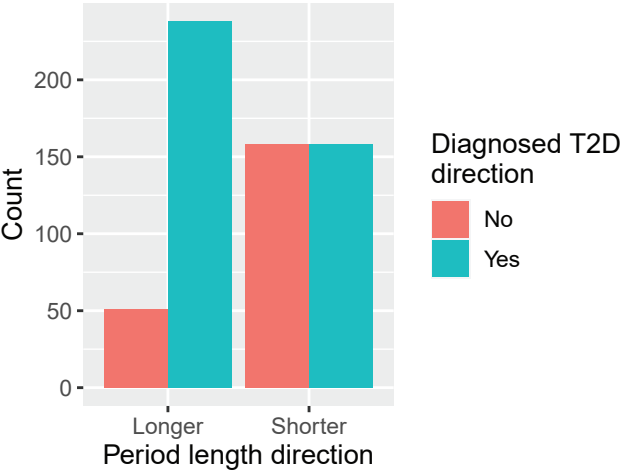
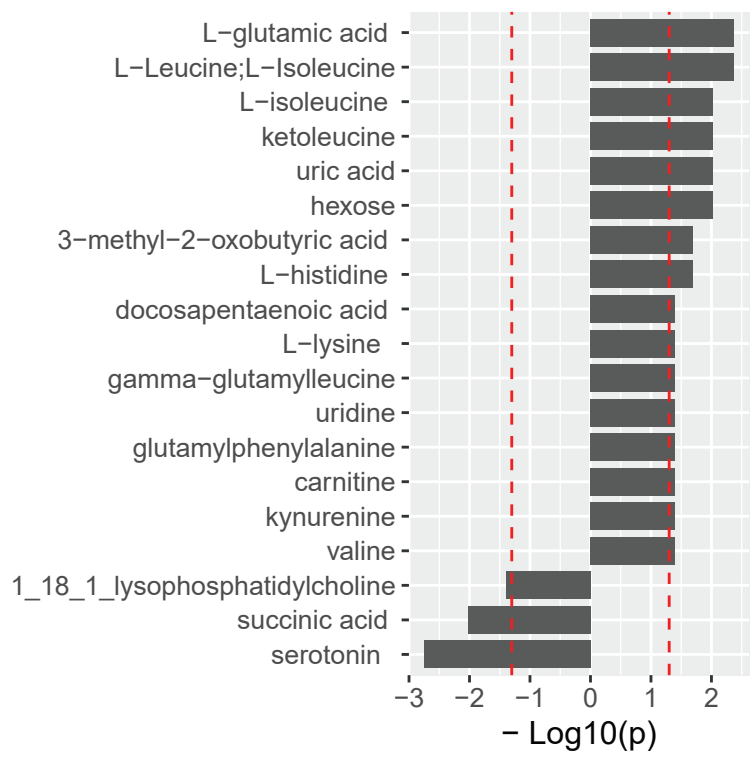
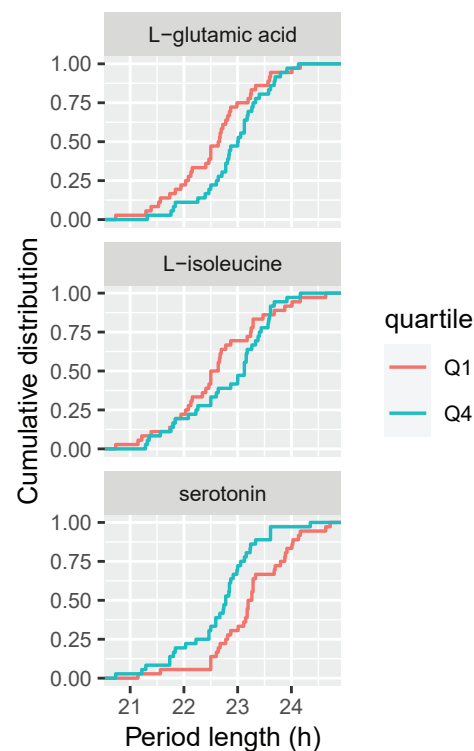


Figure 5

A



B



C

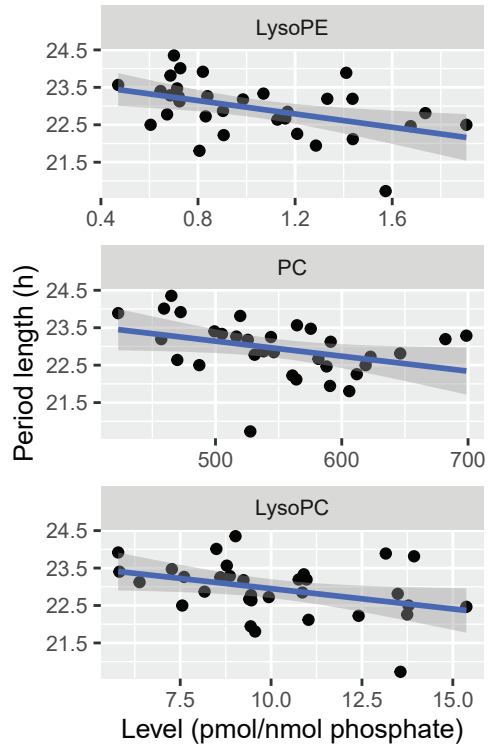
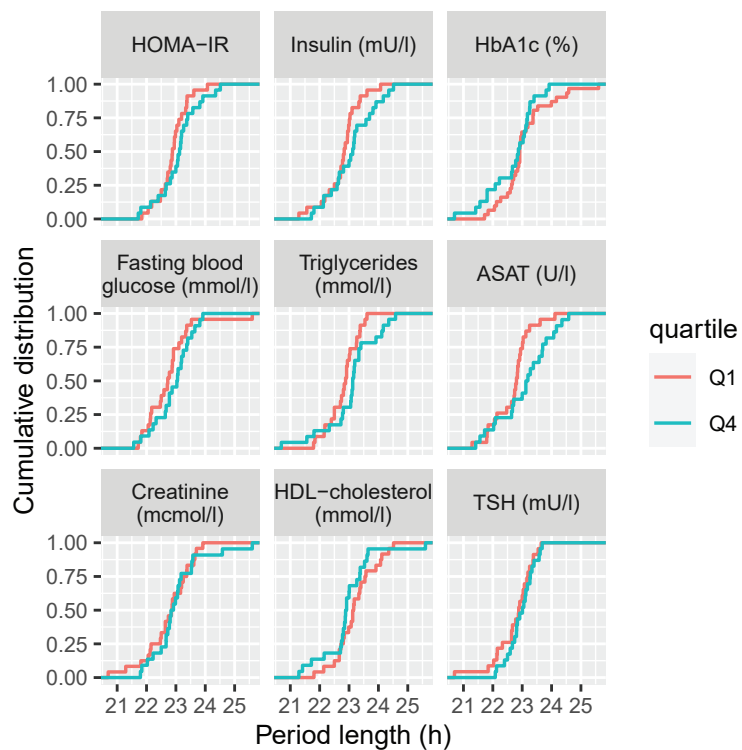


Figure S1

A



B

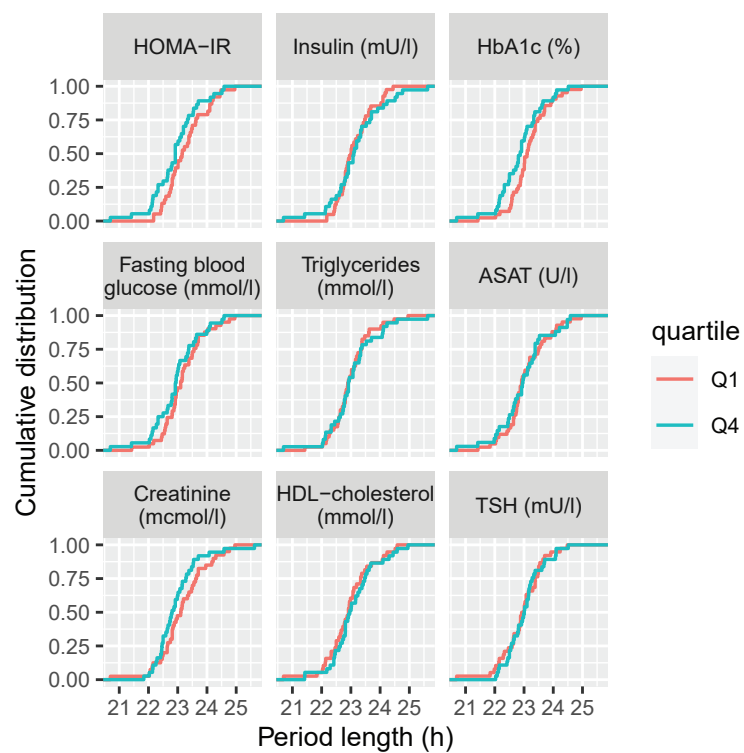
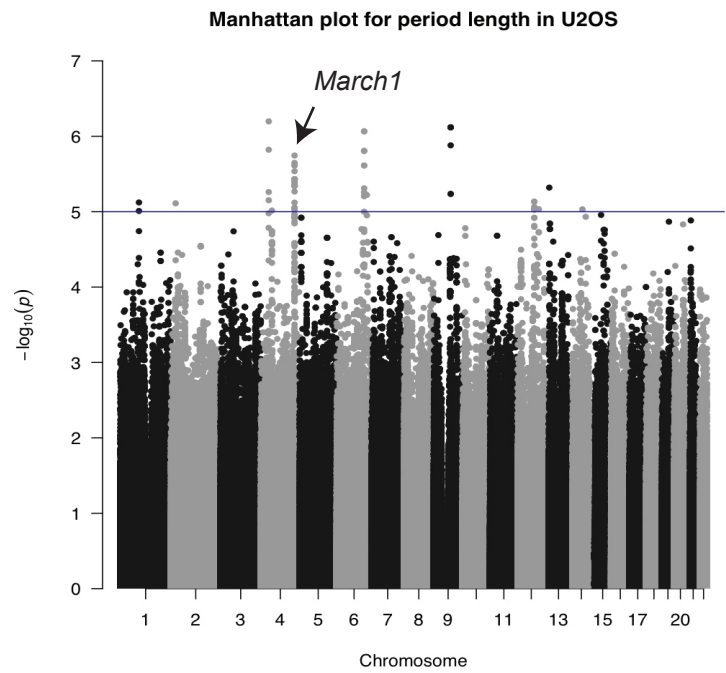


Figure S2

A



B

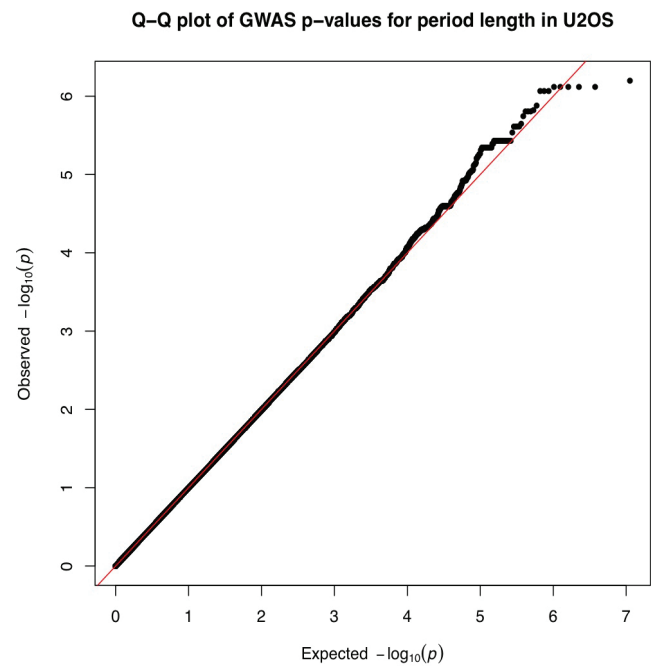
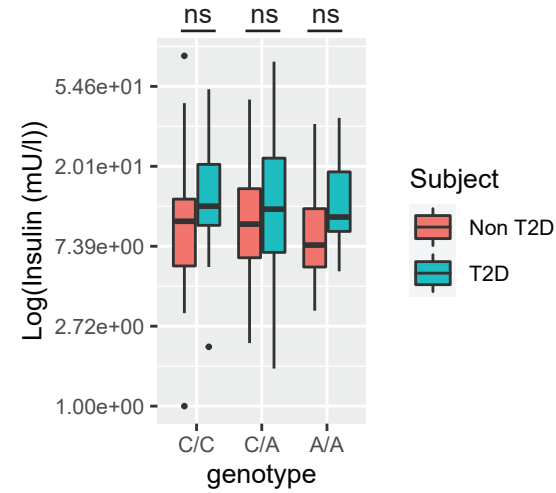


Figure S3

A



B

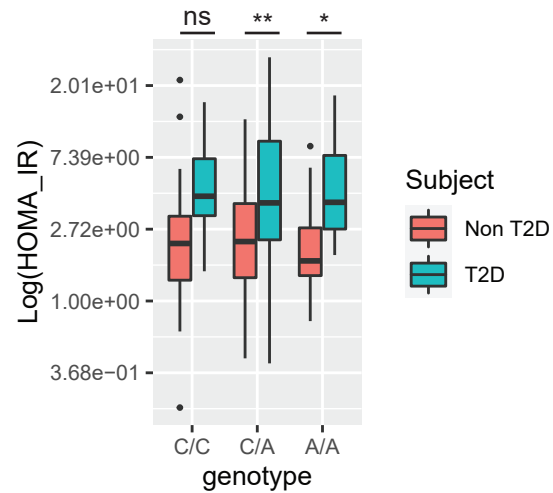
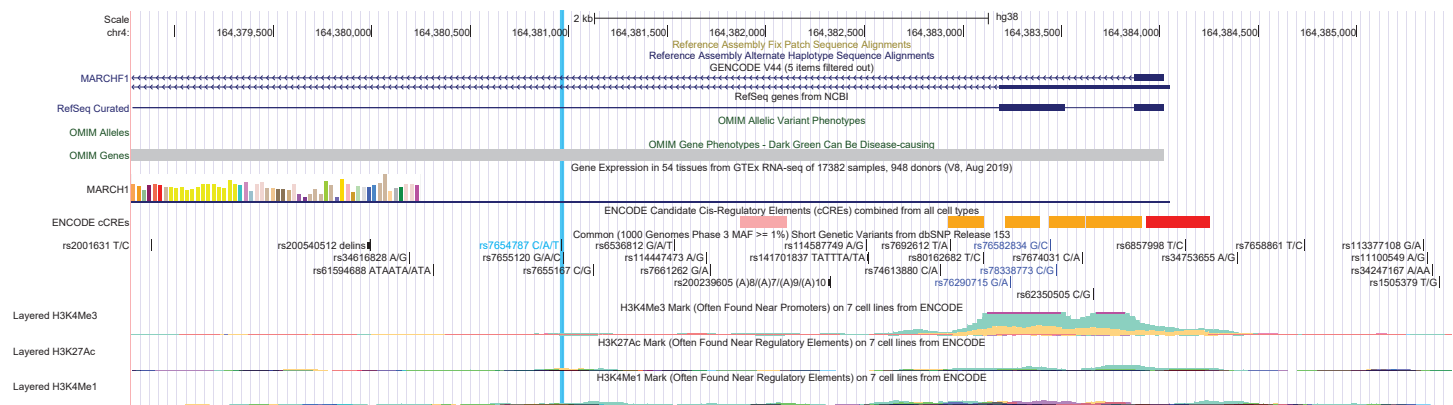


Figure S4

A



B

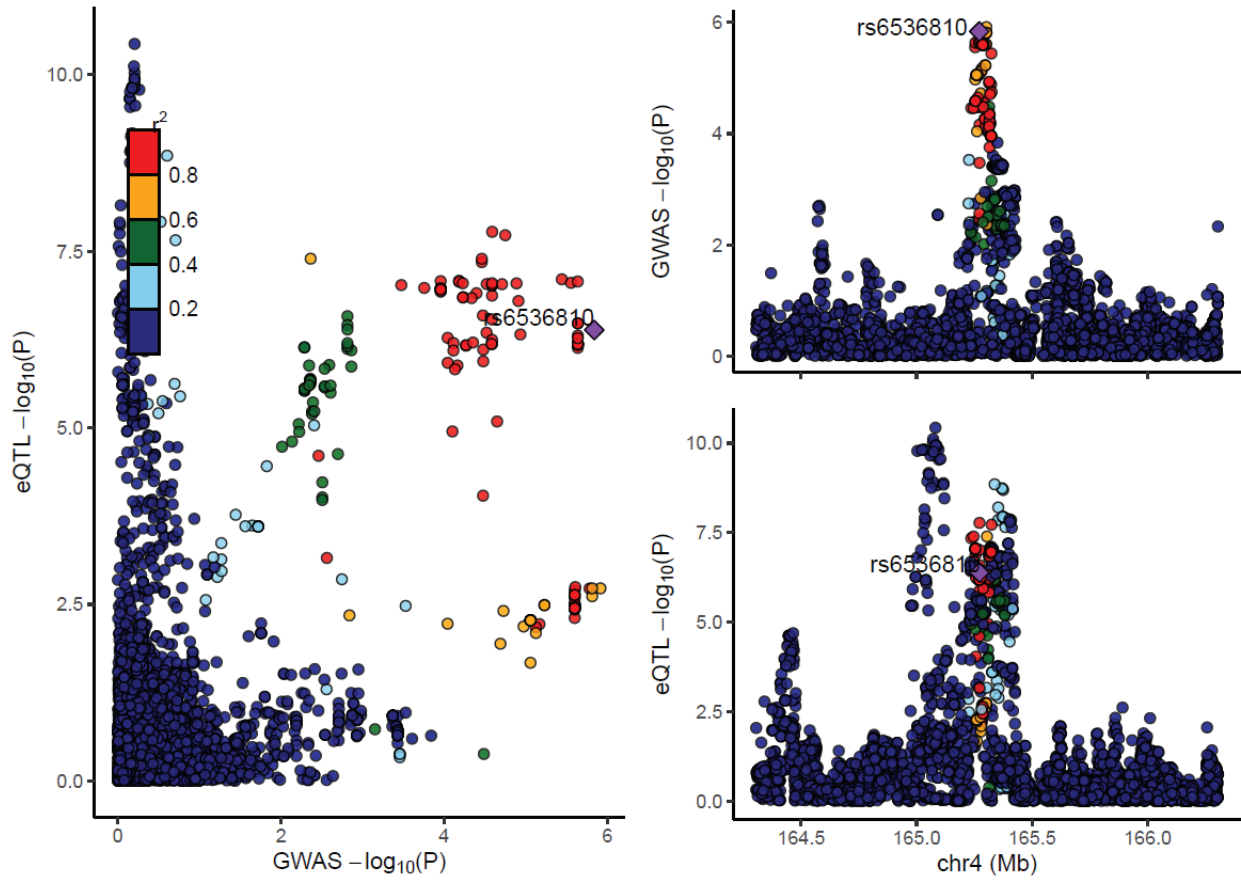


Figure S5

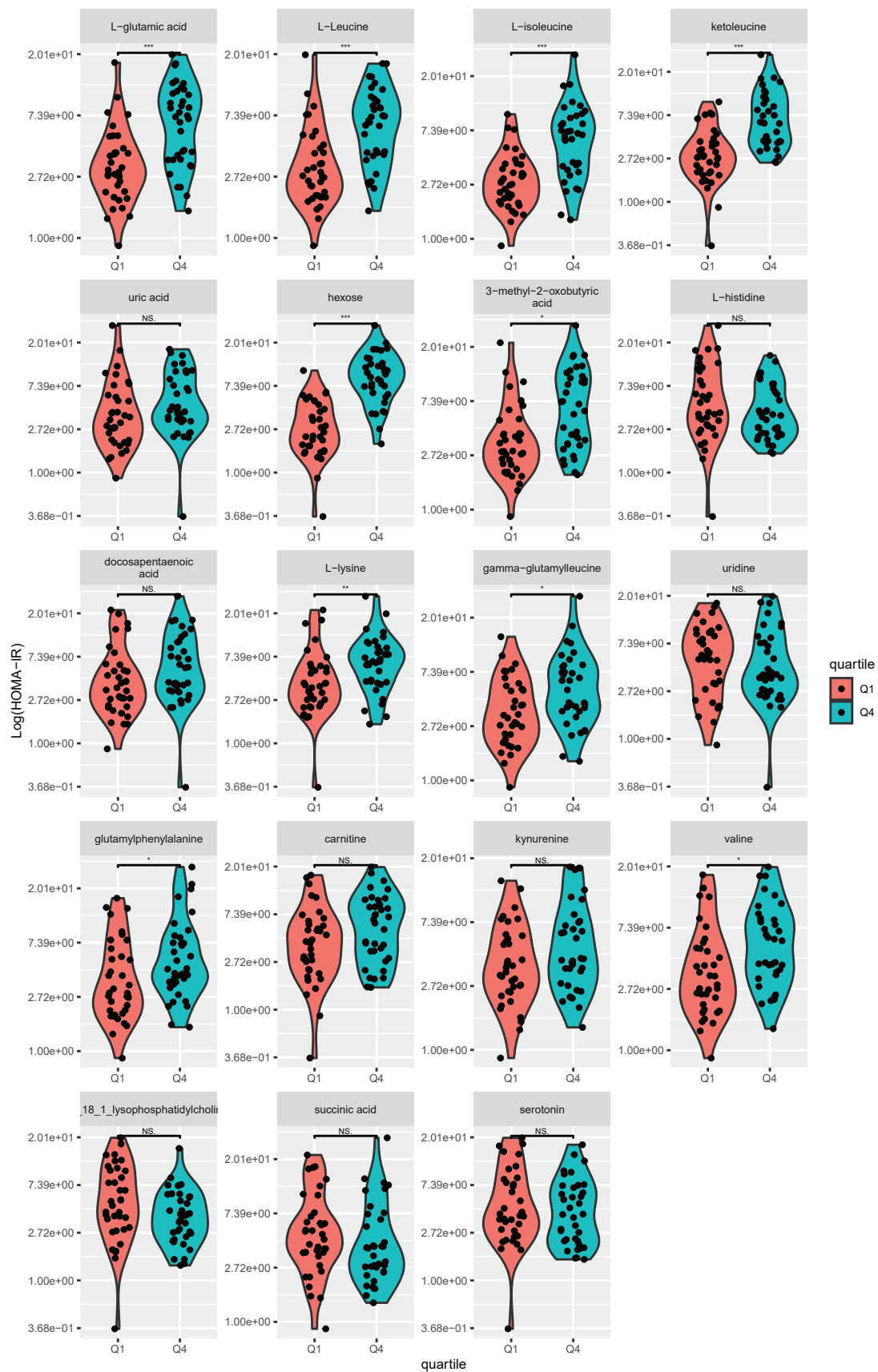
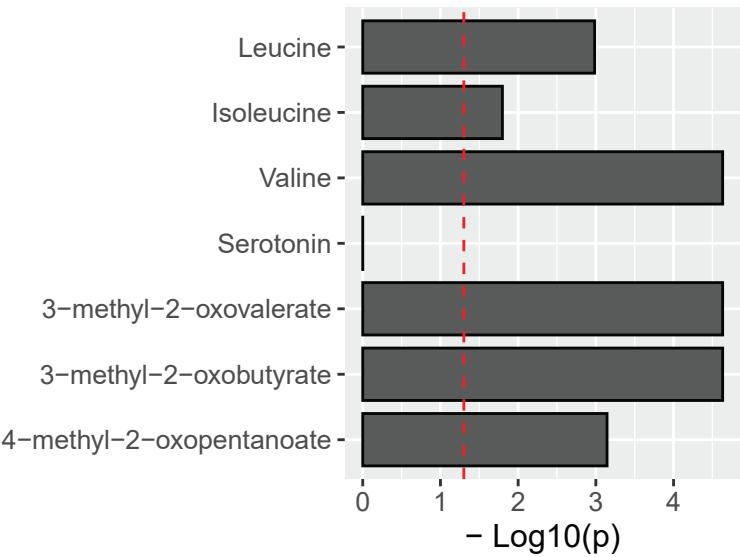


Figure S6

A



B

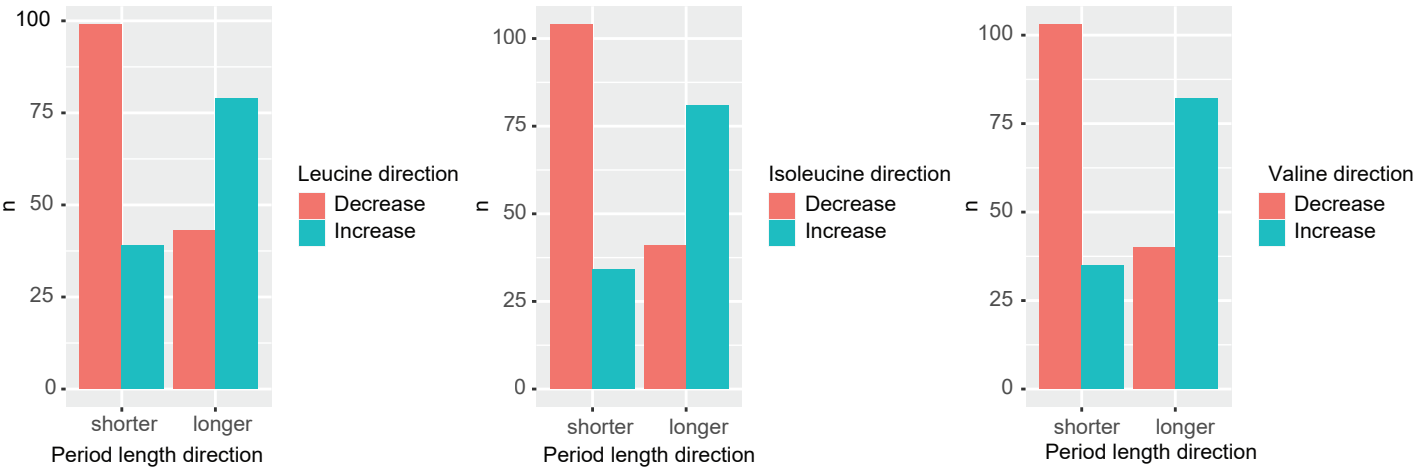
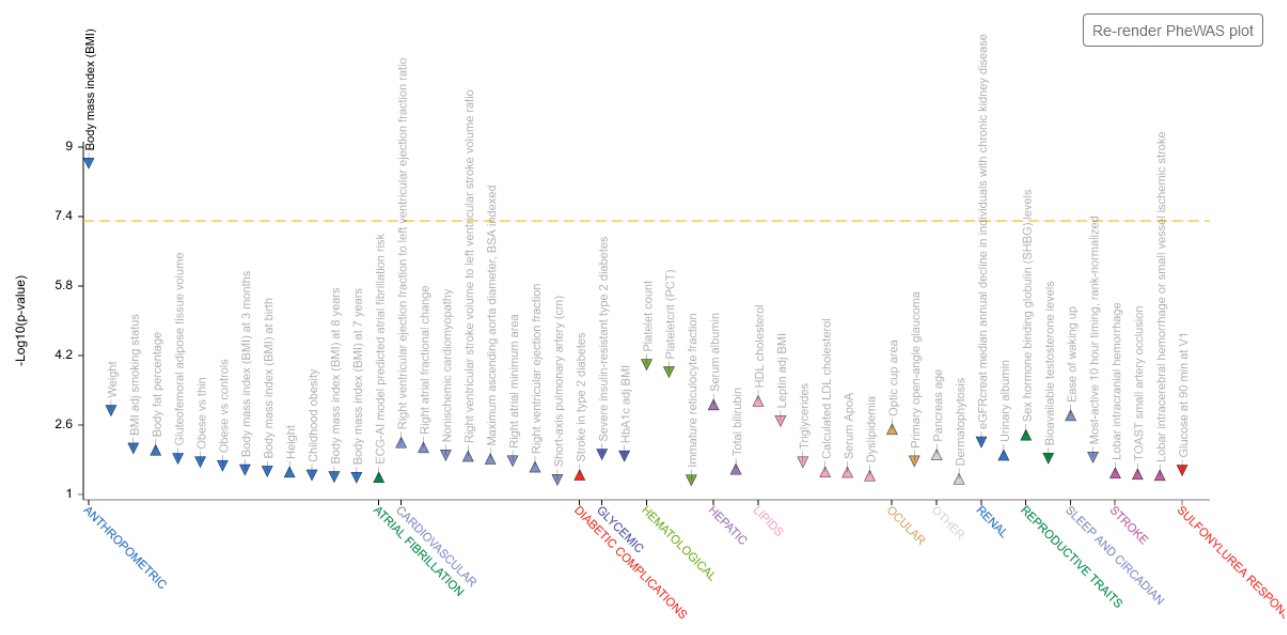


Figure S7



Phenotype	P-Value	Beta	Odds Ratio	Effective Sample Size	View
Body mass index (BMI)	2.37e-9	▼-0.0091		3,894,810	Datasets Top 25 variants
Platelet count	0.0001024	▼-0.0064		1,579,360	Datasets Top 25 variants
Plateletcrit (PCT)	0.0001518	▼-0.0068		853,969	Datasets Top 25 variants
HDL cholesterol	0.000697	▲0.0031		2,434,690	Datasets Top 25 variants
Serum albumin	0.0008504	▲0.0038		533,448	Datasets Top 25 variants
Weight	0.001171	▼-0.0055		489,228	Datasets Top 25 variants
Ease of waking up	0.0015	▲0.0051		451,872	Datasets Top 25 variants
Leptin adj BMI	0.002035	▼-0.0207		29,468	Datasets Top 25 variants
Optic cup area	0.003118	▲0.0071		22,484	Datasets Top 25 variants
Sex hormone binding globulin (SHBG) levels	0.004232	▲0.0056		1,137,690	Datasets Top 25 variants

Figure S8

